

New superexchange paths due to breathing-enhanced hopping in corner-sharing cuprates

Nikolay A. Bogdanov,¹ Giovanni Li Manni,¹ Sandeep Sharma,^{1,2} Olle Gunnarsson,¹ and Ali Alavi^{1,3}

¹Max Planck Institute for Solid State Research, Heisenbergstraße 1, 70569 Stuttgart, Germany

²Department of Chemistry and Biochemistry, University of Colorado Boulder, Boulder, Colorado 80302, USA

³University Chemical Laboratory, Lensfield Road, Cambridge, CB2 1DEW, U.K.

(Dated: March 20, 2018)

We present *ab initio* calculations of the superexchange antiferromagnetic spin coupling J for two cuprates, Sr_2CuO_3 and La_2CuO_4 . Good agreement with experimental estimates is obtained. We find that J increases substantially as the distance between Cu and apical O is increased. There is an important synergetic effect of the Coulomb interaction, expanding the Cu 3d orbital when an electron hops into this orbital, and the O-Cu hopping, being increased by this orbital expansion (breathing). This is a new ingredient in superexchange models. In a model with a fixed basis, breathing effects can be described as a mixing of 3d and 4d orbitals or as a single $3d \rightarrow 4d$ excitation.

Cuprates with corner-sharing CuO_4 plaquettes have received much attention due to discoveries of high-temperature superconductivity [1] and exotic states where spin and charge [2] or spin and orbital [3] degrees of freedom are separated. In these systems spins are coupled antiferromagnetically (AF), and it is believed that spin fluctuations play an important role. The strength of the AF coupling can be characterized by the nearest-neighbor (NN) coupling J , which enters in, e.g., the Heisenberg model for undoped systems and the t - J model for doped systems [4]. Experimentally, the magnitude of J varies strongly between different cuprates, typically in the range 0.12-0.25 eV [3, 5–8]. This variation has been assigned to the dimensionality of the Cu-O network [9] and to the distance d_{CuO} between Cu and apical O [9, 10]. Our *ab initio* calculations show that an increase of d_{CuO} leads to substantially larger J . Recent experimental work indeed finds such an increase [11].

The AF coupling in these compounds occurs via superexchange [12, 13]. This involves the (virtual) electron hopping between the Cu 3d and O 2p orbitals. Antiparallel spins on neighboring Cu atoms allow for more hopping possibilities than parallel spins, leading to an AF coupling [14, 15]. While the superexchange is well understood on the model level, the *ab initio* calculation of J is a major problem. For instance, calculations in a minimum though physically plausible basis set underestimate J by almost an order of magnitude. This is therefore a long-standing problem in the *ab initio* community [16–19].

We use wavefunction-based methods [20] relying on full configuration interaction quantum Monte Carlo (FCIQMC) [21, 22] and density-matrix renormalization group (DMRG) [23, 24] as underlying solvers and restrict the calculations to the NN J . An exact calculation within our model would involve correlating ≈ 100 electrons among ≈ 300 orbitals, leading to a eigenvalue problem in a Hilbert space of 10^{115} determinants. Since problems on such a scale are out of reach, we use the method of complete-active-space-self-

consistent-field (CASSCF) together with multi-reference perturbation theories to systematically approximate the correlation energy [25]. In the CASSCF(n,m) approach, a subset n of the electrons (the active electrons) are fully correlated among an active set of m orbitals, leading to a highly multi-configurational (CAS) reference wavefunction. The choice of the active space will be discussed shortly, but let us note that although this is still an exponential-scaling problem, it is manageable with the aforementioned techniques as long as n and m are not too large. In the SCF step, all orbitals are self-consistently optimised in the field of the multi-determinant wavefunction (WF), to yield the variational minimum. The CAS WF is then augmented using a number of second-order techniques, including n -electron perturbation theory (NEVPT2) [26, 27], multireference linearized coupled cluster (MR-LCC2) [27, 28], or multireference configuration interaction with single and double excitations (MR-CISD) [20]; these methods capture the remaining (weak) correlation involving electrons and orbitals outside of the active space. We use these different second order methods as a gauge of their reliability. As the active space is enlarged, the corresponding second-order corrections diminishes. The key question that arises is: what is the “minimal” active space necessary to obtain a qualitatively correct reference wavefunction, sufficient to compute J reliably? We find that the necessary active space needs to be far larger than previously imagined, including relatively high energy Cu 4d and O 3p orbitals. Exclusion of these states from the active spaces leads a dramatic underestimation of J .

We analyze the reason for the strong dependence of J on the active space and, in particular, the importance of 4d orbitals. As mentioned above, the superexchange mechanism depends on O-Cu hopping. The Coulomb energy cost U_{eff} of this hopping is strongly reduced by an expansion of the Cu 3d orbitals, referred to as breathing [29], when an electron hops into a Cu 3d orbital. This breathing effect at the same time increases the Cu-O ef-

fective hopping integral t_{eff} [30]. In a similar way the O 2p orbital breathes as the O occupancy is changed. In the superexchange mechanism, J depends on both U_{eff} and t_{eff} [15] and the breathing effects therefore strongly influence J . In a Hilbert space constructed with orthogonal orbitals, the breathing effect is described by the formation of linear combinations of, e.g., 3d and 4d orbitals, showing up as an increased occupancy of the 4d orbitals.

The breathing effects involve a single $3d \rightarrow 4d$ excitation, leading to an *expansion* of the charge density when an electron is added to the d shell. There are also important double $3d \rightarrow 4d$ excitations, which provide radial (in-out) correlations [20]. For a fixed number of d electrons, these correlations lead to a *contraction* of the charge density, at least if the basis has sufficient flexibility to satisfy the virial theorem. Correlation and breathing compete, making the simultaneous description complicated. Both effects lead to the occupancy of 4d orbitals, but are otherwise very different.

To study the electronic structure of cuprates we employ the embedded cluster model. With this approach accurate high-level calculation is performed for a small representative unit of the solid, while its environment is treated in a more approximate manner [31]. We use clusters that include two CuO_4 (CuO_6) units, two (ten) neighboring Cu^{2+} ions and all adjacent Sr^{2+} (La^{3+}) ions, in total $[\text{Cu}_4\text{O}_7\text{Sr}_{16}]$ and $[\text{Cu}_{12}\text{O}_{11}\text{La}_{16}]$ for Sr_2CuO_3 and La_2CuO_4 respectively. The rest of the solid is modeled by an array of point charges fitted to reproduce the Madelung potential in the cluster region [32–34]. We employed the crystal structures as reported in Refs. [35] and [36]. The value of the NN superexchange parameter can be easily extracted by mapping the energy spectrum of the two-magnetic-site cluster to two-site Heisenberg model. To make this mapping straightforward, the peripheral Cu ions are represented by total-ion potentials with no associated electrons, such that J can be extracted as the energy difference of lowest triplet and singlet states [31]. We use all electron cc-pVDZ and cc-pVTZ basis sets for central Cu and O ions [37, 38], large-core effective potentials for other species [39–41] and utilize several quantum chemistry computational packages [42–46], see supplementary material for more details [15].

We first perform CASSCF calculation with two singly occupied Cu $3d_{x^2-y^2}$ orbitals in the active-space, CASSCF(2,2) similar to the one-band Hubbard model. Such minimal active-space calculation accounts for the unscreened Anderson superexchange mechanism ($d^9 - d^9$ and $d^8 - d^{10}$ configurations) and gives a qualitatively correct AF J coupling. The value of the J obtained this way is, however, only $\approx 20\%$ as compare to the experimental data [3, 5–7], see Table I. As it can be seen, the second order corrections nearly double J , but are clearly an insufficient treatment. Such uniform behavior of the different dynamical correlation methods suggests that

TABLE I: Values of the superexchange parameters J (in meV) obtained with different methods, see the text.

	Sr_2CuO_3		La_2CuO_4
	cc-pVDZ	cc-pVTZ	cc-pVDZ
CASSCF(2,2)	37	36	34
+MR-LCC2	57	68	52
+MR-CISD	60	52	50
+NEVPT2	67	78	59
+DDCI	246 ^a	274	150 ^a
CASSCF(4,3)	39	38	35
+MR-CISD	105	93	
+NEVPT2	112	135	61
CASSCF(8,10)	70	69	50
+MR-LCC2	151	148	112
+MR-CISD	153	–	–
+NEVPT2	145	143	107
+CASPT2	260 ^a	205	139 ^a
CASSCF(24,26)	125	116	90
+MR-LCC2	252	256	145
+NEVPT2	253	262	148
experiment	249[3], 241[6]		120[7], 138[5]

^a Ref. 18, calculations performed with different clusters and basis sets

the reference CASSCF calculation is inadequate to qualitatively describe the system, and that the active space has to be enlarged. The only exception is the difference-dedicated configuration interaction (DDCI) method that gives values of J very close to experiment on top of CASSCF(2,2) reference [17, 47]. However, the DDCI is essentially a subspace of the MRCI-SD, and significant differences of J calculated by these two methods imply that the description of electronic structure given by DDCI is far from being complete.

Because an electron hopping from the bridging O σ -bonding $2p_y$ orbital to the Cu $3d_{x^2-y^2}$ plays a crucial role in the superexchange (see, e.g., Ref. 14), this orbital is an obvious candidate to add into the active space. Such CASSCF(4,3) calculation roughly corresponds to an unscreened 3-band Hubbard model. However, the obtained magnetic couplings turn out to be less than 1 meV higher compared to CASSCF(2,2). The reason is that, despite the inclusion of important ligand-hole determinants ($d^9-p^5-d^{10}$ and $d^{10}-p^4-d^{10}$), their energy is too high to be effective, as the orbital optimization is primarily driven by the dominant $d^9-p^6-d^9$ configuration [16, 18, 48]. When we include the effect of further excited determinants at 2nd-order level on top of the CASSCF(4,3) WF, J becomes significantly larger, 105 eV using MR-CISD for the Sr_2CuO_3 compound. It is still more than two times smaller than the experimental value, indicating that important details are still missing.

To give the WF flexibility for accounting the orbital relaxation in $d^8-p^6-d^{10}$ and $d^9-p^5-d^{10}$ determinants, one

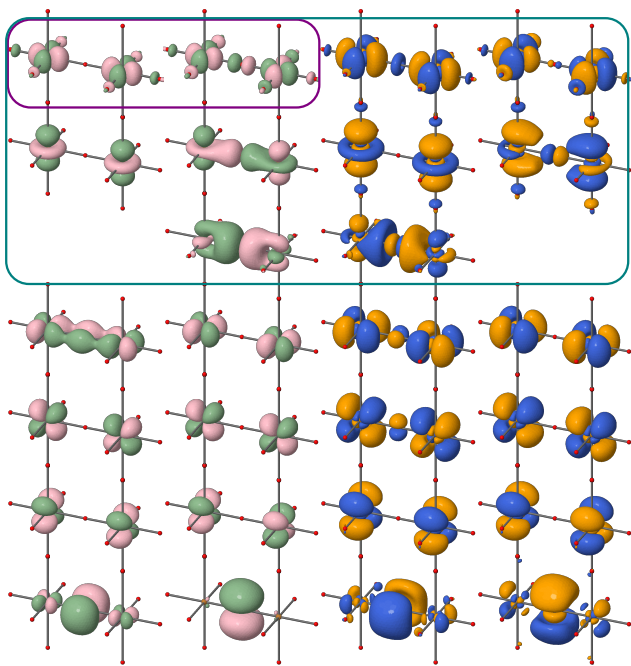


FIG. 1: Orbitals optimized in the CASSCF(24,26) calculation for the La_2CuO_4 compound. (2,2) and (8,10) subsets are indicated by smaller rectangles.

can add a set of orbitals previously kept empty (Cu 4d and O 3p) to the active space [16, 18]. Having additional d orbitals in the active space has been shown to be necessary to describe multiplet splittings for the late transition metals of the first row, see, e.g., Refs 49 and 50. Due to variability of orbital optimization within the CASSCF procedure, the active orbitals are allowed to change, and a balanced choice of active space is required to ensure convergence. Balanced active space can be constructed with Cu 3d and 4d orbitals of e_g character plus the bridging oxygen $2p_y$ and $3p_y$ orbitals [18]. Results for the CASSCF(8,10) calculations are shown in the third block of the Table I. The extension of the active space leads to a systematic differential effect, J significantly increases at all levels of theory. Results close to experiment were reported using this active space together with a different formulation of the perturbation theory [18]. But our calculations give 60 and 80 % of the experimental values for the Sr and La cuprates respectively. To get the balanced description of all relevant effects we add all copper 3d and 4d together with the bridging oxygen 2p and 3p orbitals, resulting in CASSCF(24,26). This active space yields diagonalization problem in the space of $\approx 10^{14}$ Slater determinants and is not feasible with conventional diagonalization methods, therefore we have to proceed with DMRG and FCIQMC as approximate solvers [15, 24, 51]. With the additional many-body contribution from the Cu t_{2g} and π -bonding O orbitals taken into account in the large

CASSCF we find further stabilization of the singlet compared to the triplet. Second order correction on top of the CASSCF(24,26) reference finally brings J close to the experimental values, see the last block in Table I. Orbitals as optimized in the variational calculation are shown in Figure 1. One can notice that both 3d and 4d orbitals have significant amplitudes at the bridging oxygen p orbitals.

In the standard theory [12, 13] of superexchange, a model of Cu_2O is treated, with one nondegenerate orbital on each atom. As discussed above, including only these orbitals in CASSCF(4,3) underestimates J by almost one order of magnitude. We now discuss why it is necessary to consider the large active space.

In calculations for the singlet and triplet states, the configuration $d^9-p^6-d^9$ dominates, and correlation effects in this configuration are very important for the total energy. However, the contributions for the singlet and triplet states are similar and therefore not very important for J . In superexchange theory, hopping of electrons between Cu and O plays a crucial role, involving, e.g., d^8-d^{10} determinants in addition to the nominal d^9-d^9 . There are more configurations of this type available for the singlet than the triplet state. Although these configurations have rather small weights, they are crucial for J . These configurations are indicated in the supplementary material [15].

The on-site Coulomb integral between two 3d electrons is very large (≈ 28 eV [52]), leading to drastically suppressed charge fluctuations in the simplest model. This is the reason the CASSCF(2,2) and CASSCF(4,3) give a very small J . However, by increasing the active space size, this energy cost can be strongly reduced. Crucial effects are the change of the effective radial extent of the 3d orbital (breathing) and rearrangements of the non-3d charge density as the number of 3d electrons varies (screening) [29], which are captured in the CASSCF(24,26) calculation with second-order correction.

In order to disentangle these different effects we performed a series of simpler constrained calculations [15, 53]. We put all hopping integrals from d (3d or 4d) basis functions on the Cu atoms equal to zero. We can then prescribe the total occupancy of d orbitals on each Cu atom. We performed two calculations, one with the configurations d^9-d^9 and one with d^8-d^{10} . In both cases the system is allowed to fully relax, except that hopping to or from d orbitals is suppressed. We then obtain that the energy for the d^8-d^{10} state is about 12 eV higher than for d^9-d^9 . This means that $U \approx 28$ eV has been reduced to $U_{\text{eff}} \approx 12$ eV. According to other estimates, U_{eff} is reduced even further (≈ 8 eV [54]).

Figure 2 shows charge differences due to breathing and screening for the d^8-d^{10} calculation, discussed above. A calculation was first performed for d^9-d^9 , then a d electron was moved from one Cu atom to the

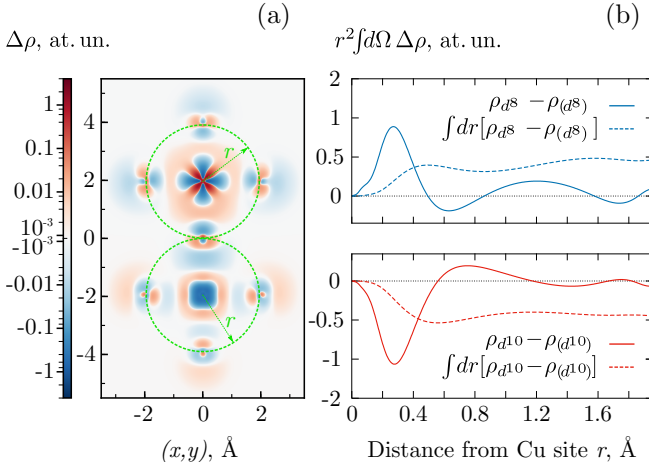


FIG. 2: Electron density difference due to orbital relaxation in the $d^8 - d^{10}$ configuration. (a) In the plane of CuO_4 plaquettes; (b) integrated over a sphere centered on one of the Cu atoms (full curves) as a function of the radius as shown in (a). The results of an additional radial integration are shown by the dashed curves as a function of the upper integration limit.

other keeping all orbitals unchanged. The corresponding densities are denoted $\rho_{(d^8)}$ and $\rho_{(d^{10})}$. This $d^8 - d^{10}$ state was then allowed to relax self-consistently, giving the densities ρ_{d^8} and $\rho_{d^{10}}$. The full red curve shows the change in charge density $\rho_{d^{10}} - \rho_{(d^{10})}$, illustrating how charge is moved from the inner part of Cu to the outer part (breathing). The red dashed curve shows a radial integral of the charge density difference. It shows that more charge is removed from the inner part than added to the outer part. Since the number of d-electrons is the same in the two calculations, non-d charge has been moved away from the Cu atom with the d^{10} configurations as a response to the addition of one d electrons (screening). Adding a d electron to a Cu atom then only leads to an increase of the net charge by about half an electron, due to screening, which substantially reduces the energy cost.

As in can be seen in Table I, magnetic coupling in Sr_2CuO_3 is nearly two times larger than in La_2CuO_4 . In both cases the computation of J is done using only two magnetic centers, therefore this difference should not be attributed to dimensionality of two materials. The other structural difference is the presence of apical oxygen ions in the La_2CuO_4 that changes the local multiplet splittings, mainly the position of $3d_{z^2}$ levels [3, 55–57]. Relative energy of $3d_{z^2}$ orbital is believed to be connected to the shape of the Fermi surface and the value of the critical temperature in doped cuprates [58–61].

There are experimental evidences that J also changes depending on the local geometry [8]. However, because experimentally different compounds have to be used,

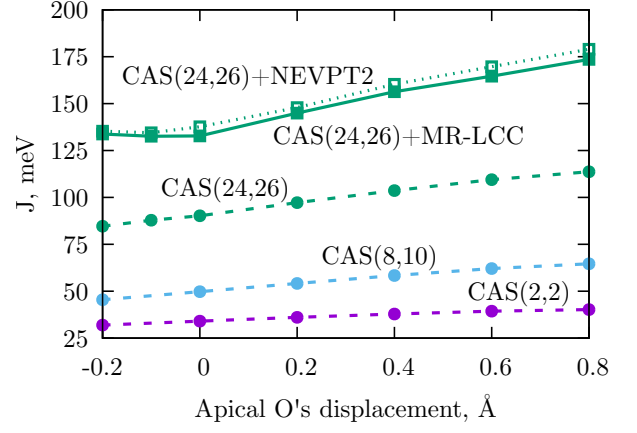


FIG. 3: Dependence of J on the distance to apical oxygens in La_2CuO_4 .

local distortions are accompanied by changes of Cu–O distances and type of adjacent metal ions. Therefore it is instructive to investigate the dependence of J on the distance to apical oxygen ions in La_2CuO_4 compound with accurate computational method. We varied the apical O's positions within the cluster keeping the electrostatic potential untouched and compute magnetic couplings using the procedure described above. The results of these calculations are presented in Figure 3. It can be seen that with increase of the distance to apical oxygen the NN J grows. It shows that the growth is faster with more electron correlation is taken into account. One obvious effect that leads to increase of J is the lowering of the $4d_{z^2}$ orbital energy and corresponding enhancement the orbital breathing: we observe 13% growth of the occupation of $4d_{z^2}$ orbitals upon 0.8 Å displacement of apical oxygens at the CASSCF(24,26) level. Recent experimental results for J in thin films is in good agreement with our calculations [11].

In this letter we presented state-of-the are *ab initio* calculations of the NN magnetic coupling in cuprate compounds. We find that orbital breathing involving Cu 4d orbitals is essential to properly describe magnetism in these materials. We find that a synergistic coupling between orbital breathing and enhanced hopping lead to the observed J . This mechanism also leads to a strong dependence of J on the distance to apical oxygen ions, where a 30% increase of the coupling occurs under 30% elongation of the Cu–O distance. More generally, breathing-enhanced hopping may be expected to play an important role in generating longer range hopping and exchange interactions, beyond nearest neighbors. Significant long range hopping would provide a mechanism to generate frustration on the square lattice, and in the doped cuprates may be relevant in the mechanism leading to superconductivity. These questions are left for a future study.

-
- [1] J. G. Bednorz and K. A. Müller, *Z. Phys. B* **64**, 189 (1986).
- [2] C. Kim, Z.-X. Shen, N. Motoyama, H. Eisaki, S. Uchida, T. and S. Maekawa, *Phys. Rev. B* **56**, 15589 (1997).
- [3] J. Schlappa, K. Wohlfeld, K. J. Zhou, M. Mourigal, M. W. Haverkort, V. N. Strocov, L. Hozoi, C. Monney, S. Nishimoto, S. Singh, A. Revcolevschi, J.-S. Caux, L. Patthey, H. M. Ronnow, J. van den Brink, and T. Schmitt, *Nature* **485**, 82 (2012).
- [4] F. C. Zhang and T. M. Rice, *Phys. Rev. B* **37**, 3759 (1988).
- [5] R. Coldea, S. M. Hayden, G. Aeppli, T. G. Perring, C. D. Frost, T. E. Mason, S.-W. Cheong, and Z. Fisk, *Phys. Rev. Lett.* **86**, 5377 (2001).
- [6] A. C. Walters, T. G. Perring, J.-S. Caux, A. T. Savici, G. D. Gu, C.-C. Lee, W. Ku, and I. A. Zaliznyak, *Nat. Phys.* **5**, 867 (2009).
- [7] L. Braicovich, L. J. P. Ament, V. Bisogni, F. Forte, C. Aruta, G. Balestrino, N. B. Brookes, G. M. De Luca, P. G. Medaglia, F. M. Granozio, M. Radovic, M. Salluzzo, J. van den Brink, and G. Ghiringhelli, *Phys. Rev. Lett.* **102**, 167401 (2009).
- [8] Y. Y. Peng, G. Dellea, M. Minola, M. Conni, A. Amorese, D. Di Castro, G. M. De Luca, K. Kummer, M. Salluzzo, X. Sun, X. J. Zhou, G. Balestrino, M. Le Tacon, B. Keimer, L. Braicovich, N. B. Brookes, and G. Ghiringhelli, *Nat. Phys.* **13**, 1201 (2017).
- [9] Y. Mizuno, T. Tohyama, and S. Maekawa, *Phys. Rev. B* **58**, R14713 (1998).
- [10] C. Weber, C. Yee, K. Haule, and G. Kotliar, *Europhys. Lett.* **100**, 37001 (2012).
- [11] B. Keimer *et al.*, to be published.
- [12] H. A. Kramers, *Physica* **1**, 182 (1934).
- [13] P. W. Anderson, *Phys. Rev.* **79**, 350 (1950).
- [14] D. I. Khomskii, *Transition Metal Compounds* (Cambridge University Press, 2014).
- [15] See supplementary material.
- [16] A. van Oosten, R. Broer, and W. Nieuwpoort, *Chem. Phys. Lett.* **257**, 207 (1996).
- [17] C. J. Calzado, C. Angeli, D. Taratiel, R. Caballol, and J.-P. Malrieu, *J. Chem. Phys.* **131**, 044327 (2009).
- [18] C. de Graaf, C. Sousa, I. d. P. R. Moreira, and F. Illas, *J. Phys. Chem. A* **105**, 11371 (2001).
- [19] K. Fink and V. Staemmler, *Mol. Phys.* **111**, 2594 (2013).
- [20] T. Helgaker, P. Jørgensen, and J. Olsen, *Molecular electronic-structure theory* (Wiley, Chichester, 2000).
- [21] G. H. Booth, A. J. W. Thom, and A. Alavi, *J. Chem. Phys.* **131**, 054106 (2009).
- [22] D. M. Cleland, G. H. Booth, and A. Alavi, *J. Chem. Phys.* **134**, 024112 (2011).
- [23] S. Sharma and G. K.-L. Chan, *J. Chem. Phys.* **136**, 124121 (2012).
- [24] Q. Sun, J. Yang, and G. K.-L. Chan, *Chem. Phys. Lett.* **683**, 291 (2017).
- [25] B. O. Roos, P. R. Taylor, and P. E. Siegbahn, *Chem. Phys.* **48**, 157 (1980).
- [26] C. Angeli, R. Cimiraglia, and J.-P. Malrieu, *Chem. Phys. Lett.* **350**, 297 (2001).
- [27] S. Sharma, G. Knizia, S. Guo, and A. Alavi, *J. Chem. Theory Comput.* **13**, 488 (2017).
- [28] S. Sharma and A. Alavi, *J. Chem. Phys.* **143**, 102815 (2015).
- [29] O. Gunnarsson, O. K. Andersen, O. Jepsen, and J. Zaanen, *Phys. Rev. B* **39**, 1708 (1989).
- [30] O. Gunnarsson and O. Jepsen, *Phys. Rev. B* **38**, 3568(R) (1988).
- [31] C. de Graaf and R. Broer, *Magnetic Interactions in Molecules and Solids* (Springer Int. Pub., 2016).
- [32] P. P. Ewald, *Ann. Phys.* **369**, 253 (1921).
- [33] M. Klintonberg, S. Derenzo, and M. Weber, *Comput. Phys. Commun.* **131**, 120 (2000).
- [34] B. Roos and U. Wahlgren, "MADPOT and MADFIT programs," Institute of Theoretical Physics, University of Stockholm (1969).
- [35] N. C. Hyatt, L. Gray, I. Gameson, P. P. Edwards, and S. Hull, *Phys. Rev. B* **70**, 214101 (2004).
- [36] P. G. Radaelli, D. G. Hinks, A. W. Mitchell, B. A. Hunter, J. L. Wagner, B. Dabrowski, K. G. Vandervoort, H. K. Viswanathan, and J. D. Jorgensen, *Phys. Rev. B* **49**, 4163 (1994).
- [37] T. H. Dunning Jr., *J. Chem. Phys.* **90**, 1007 (1989).
- [38] N. B. Balabanov and K. A. Peterson, *J. Chem. Phys.* **123**, 064107 (2005).
- [39] P. Fuentealba, L. von Szentpály, H. Preuss, and H. Stoll, *J. Phys. B* **18**, 1287 (1985).
- [40] M. Dolg, H. Stoll, A. Savin, and H. Preuss, *Theor. Chim. Acta* **75**, 173 (1989).
- [41] M. Dolg, H. Stoll, and H. Preuss, *Theor. Chim. Acta* **85**, 441 (1993).
- [42] G. H. Booth, S. D. Smart, and A. Alavi, *Mol. Phys.* **112**, 1855 (2014).
- [43] F. Aquilante, J. Autschbach, R. K. Carlson, L. F. Chibotaru, M. G. Delcey, L. De Vico, I. Fdez. Galván, N. Ferré, L. M. Frutos, L. Gagliardi, M. Garavelli, A. Giussani, C. E. Hoyer, G. Li Manni, H. Lischka, D. Ma, P. Å. Malmqvist, T. Müller, A. Nenov, M. Olivucci, T. B. Pedersen, D. Peng, F. Plasser, B. Pritchard, M. Reiher, I. Rivalta, I. Schapiro, J. Segarra-Martí, M. Stenrup, D. G. Truhlar, L. Ungur, A. Valentini, S. Vancoillie, V. Veryazov, V. P. Vysotskiy, O. Weingart, F. Zapata, and R. Lindh, *J. Comput. Chem.* **37**, 506 (2015).
- [44] Q. Sun, T. C. Berkelbach, N. S. Blunt, G. H. Booth, S. Guo, Z. Li, J. Liu, J. D. McClain, E. R. Sayfutyarova, S. Sharma, S. Wouters, and G. K.-L. Chan, *WIREs Comput. Mol. Sci.* **8**, e1340 (2017).
- [45] H.-J. Werner, P. J. Knowles, G. Knizia, F. R. Manby, and M. Schütz, *WIREs Comput. Mol. Sci.* **2**, 242 (2011).
- [46] H. Lischka, T. Müller, P. G. Szalay, I. Shavitt, R. M. Pitzer, and R. Shepard, *WIREs Comput. Mol. Sci.* **1**, 191 (2011).
- [47] DDCI was developed as a method for calculating magnetic couplings, it was justified using the second-order perturbation theory to take into account most of the relevant physical effects (see, e.g., Refs. 17 and 48).
- [48] J. P. Malrieu, R. Caballol, C. J. Calzado, C. de Graaf, and N. Guihéry, *Chem. Rev.* **114**, 429 (2013).
- [49] K. Andersson and B. O. Roos, *Chem. Phys. Lett.* **191**, 507 (1992).
- [50] K. Pierloot, *Int. J. Quantum Chem.* **111**, 3291 (2011).
- [51] G. Li Manni, S. D. Smart, and A. Alavi, *J. Chem. Theory Comput.* **12**, 1245 (2016).
- [52] Computed as $U = 2E_{d^9} - E_{d^8} - E_{d^{10}}$ for Cu ion at CASCI level with 9, 8 and 10 electrons in 5 orbitals optimized for the d^9 state. Bare Coulomb integral $\langle 3d3d || 3d3d \rangle$ is 29.8 eV in these calculations.
- [53] D. Ma, G. Li Manni, and L. Gagliardi, *J. Chem. Phys.* **135**, 044128 (2011).
- [54] O. Gunnarsson, O. Jepsen, and Z.-X. Shen, *Phys. Rev. B*

- [42](#), 8707 (1990).
- [55] M. Moretti Sala, V. Bisogni, C. Aruta, G. Balestrino, H. Berger, N. B. Brookes, G. M. de Luca, D. Di Castro, M. Grioni, M. Guarise, P. G. Medaglia, F. Miletto Granozio, M. Minola, P. Perna, M. Radovic, M. Salluzzo, T. Schmitt, K. J. Zhou, L. Braicovich, and G. Ghiringhelli, [New J. Phys.](#) **13**, 043026 (2011).
 - [56] L. Hozoi, L. Siurakshina, P. Fulde, and J. van den Brink, [Scientific Reports](#) **1**, 65 (2011).
 - [57] H.-Y. Huang, N. A. Bogdanov, L. Siurakshina, P. Fulde, J. van den Brink, and L. Hozoi, [Phys. Rev. B](#) **84**, 235125 (2011).
 - [58] H. Eskes and G. A. Sawatzky, [Phys. Rev. B](#) **44**, 9656 (1991).
 - [59] Y. Ohta, T. Tohyama, and S. Maekawa, [Phys. Rev. B](#) **43**, 2968 (1991).
 - [60] R. Raimondi, J. H. Jefferson, and L. F. Feiner, [Phys. Rev. B](#) **53**, 8774 (1996).
 - [61] L. Hozoi, M. S. Laad, and P. Fulde, [Phys. Rev. B](#) **78**, 165107 (2008).
 - [62] T. Lu and F. Chen, [J. Comput. Chem.](#) **33**, 580 (2012).
 - [63] Jmol: an open-source Java viewer for chemical structures in 3D. <http://www.jmol.org/>.

SUPPLEMENTARY MATERIAL

DETAILS OF CALCULATIONS

For small CASSCF calculations up to (8,10) active space were done with MOLCAS, MOLPRO and PySCF programs [43–45]. Results by different codes are fully consistent, differences of total energies were not more than 10^{-6} Hartree. All NEVPT2 and MR-LCC2 calculations were carried out with IC-MPS-PT and BLOCK programs [23, 27]. MRCI-SD calculations were done using COLUMBUS and MOLCAS driver [43, 46]. CASPT2 calculations were performed with MOLCAS 8 [43]. DDCI calculations were done with MRCI module of MOLPRO [45]. Large CASSCF(24,26) calculations were carried out with CASSCF module of MOLCAS using NECI as a

solver [42, 43, 51] and independently with PySCF using BLOCK as a solver [23, 44].

Data shown in Fig. 2 was obtained in constrained calculations using generalized active space SCF (GASSCF) method as implemented in MOLCAS [43, 53]. We split atomic-like orbitals in three groups: all d orbitals at the first copper ion (15 in cc-pVDZ basis), all d orbitals at the second copper ion (15), and the rest. Any orbital rotation between these groups are forbidden via supersymmetry constrain. With GASSCF we specify two disconnected active spaces, e.g., (8,5) and (10,5) for the first and the second Cu ion respectively. This way we can fix occupation of d orbitals at each site and perform all the possible remaining optimizations.

Density plots were done with the Multiwfn program [62]. Molecular orbitals were plotted with Jmol [63].

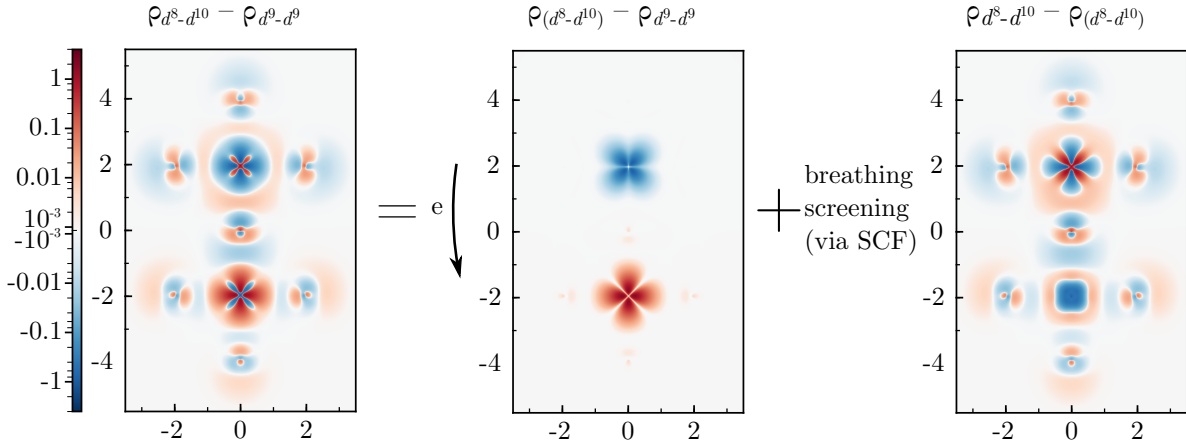


FIG. S1: Electron density differences as obtained from constrained calculations for Sr_2CuO_3 .

Clusters used in calculations are shown in Fig. S2 and Fig. S3, both belong to the D_{2h} point group. In calculations with MOLCAS, NECI, COLUMBUS, PySCF, and BLOCK were done within the full point-group symmetry. Irreducible-representation composition of active orbitals reads CAS(2,2): $[1a_g, 1b_{2u}]$; CAS(4,3): $[1a_g, 2b_{2u}]$; CAS(8,10): $[4a_g, 6b_{2u}]$; CAS(24,26): $[4a_g, 2b_{1g}, 2b_{2g}, 2b_{3g}, 2a_u, 4b_{1u}, 6b_{2u}, 4b_{3u}]$. In our setting the Cu-O-Cu link is along the y direction. Due to technical limitations calculations with MOLPRO were done within the C_1 point group.

All NEVPT2, MR-LCC2, and MRCI calculations were done correlating all Cu d and O p electrons, which is in total 60 and 84 electrons for Sr_2CuO_3 and La_2CuO_4 respectively.

To illustrate better the constrained GASSCF calculations presented in the main text we show in Fig. S1 electron density differences between three states. We start with fully optimized $d^9 - d^9$ state, then obtain $(d^8 - d^{10})$ state by moving an electron from one Cu site to the other keeping the orbitals untouched, and finally reach

the $d^8 - d^{10}$ state after orbital relaxation that captures breathing and screening. One should notice that in both latter states multiplet effects at the d^8 site are taken into account by including all determinants that arise by distributing 8 electrons in five d orbitals into the WF expansion. This multiplet effects lead to ≈ 1 eV reduction of the U_{eff} .

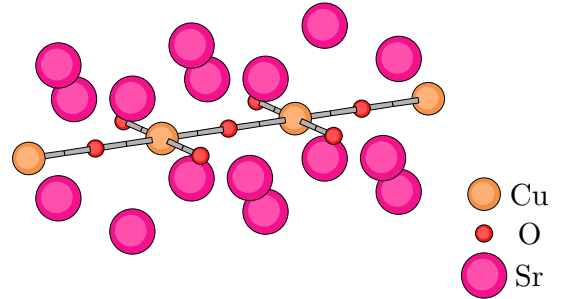


FIG. S2: Sketch of the $[\text{Cu}_4\text{O}_7\text{Sr}_{16}]$ cluster used in calculations of the Sr_2CuO_3 compound.

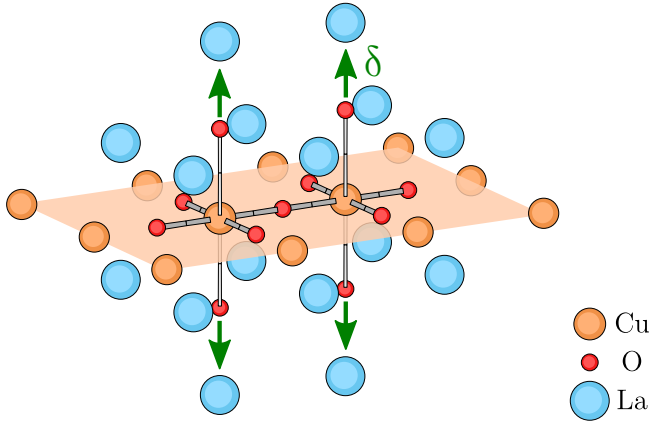


FIG. S3: Sketch of the $[\text{Cu}_{12}\text{O}_{11}\text{La}_{16}]$ cluster used in calculations of the La_2CuO_4 compound. Green arrows represent the apical oxygen displacements discussed in the main text.

BREATHING IN A Cu_2 MODEL

In this section we discuss breathing in a very simple Cu_2 model, with an effective hopping directly between two Cu atoms rather than via bridging O. We show how the radial extent of the Cu 3d orbital is effectively increased in intermediate states with increased 3d occupancy. This has two important consequences. First, the effective energy cost of increasing the occupancy of 3d level is reduced, since the electrons can avoid each other better[29]. Second, the hopping between the two sites is enhanced, as the Cu 3d orbital expands[30].

In the CASSCF calculations in the main text, a fixed orthogonal basis set is used for all intermediate states. Therefore the breathing effect of a 3d orbital is then described as a mixing of the 3d and 4d orbitals. The system can then effectively expand or contract an effective 3d orbital, depending on the relative sign of the mixing. To illustrate how this happens we consider a Cu_2 dimer, including just one 3d and one 4d level on each atom, as indicated in Fig. S4. The levels have spin but no orbital degeneracy. We use the Hamiltonian

$$H = \sum_{\sigma} \left[\sum_{i=1}^2 \sum_{j=1}^2 \varepsilon_j n_{ij\sigma} + \sum_{i=1}^2 \sum_{j=1}^2 t_{ij} (c_{1i\sigma}^{\dagger} c_{2j\sigma} + c_{2i\sigma}^{\dagger} c_{1j\sigma}) \right] + \sum_{i=1}^2 \left[U_{11} n_{i1\uparrow} n_{i1\downarrow} + U_{22} n_{i2\uparrow} n_{i2\downarrow} + U_{12} \sum_{\sigma\sigma'} n_{i1\sigma} n_{i2\sigma'} \right] + \sum_{i=1}^2 \sum_{\sigma} (K_1 n_{i1\sigma} + K_2 n_{i2\sigma}) (c_{i1-\sigma}^{\dagger} c_{i2-\sigma} + c_{i2-\sigma}^{\dagger} c_{i1-\sigma}). \quad (\text{S1})$$

Here the first index on $c_{ij\sigma}$ refers to the site and the second labels the orbital, i.e., $j = 1(2)$ refers to a 3d (4d) orbital. The hopping between the Cu atoms is described by t_{ij} . We also include the direct on-site Coulomb integrals U_{11} , U_{12} and U_{22} , describing 3d – 3d, 3d – 4d and 4d – 4d interaction, respectively. K_i refers to a Coulomb integral with three equal orbitals and the fourth different:

$$K_i = e^2 \int d^3r \int d^3r' \frac{\phi_i(\mathbf{r})^2 \phi_1(\mathbf{r}') \phi_2(\mathbf{r}')}{|\mathbf{r} - \mathbf{r}'|}. \quad (\text{S2})$$

These integrals are crucial for the breathing effect. If, e.g., the 3d orbital on an atom is doubly occupied, the last term in Eq. (S1) can excite a single electron from the 3d orbital to the 4d orbital. For radial (in-out) correlation it is important to include terms where two 3d electrons are excited to the 4d level. Such terms are neglected here.

For simplicity, we here put $t_{12} = t_{21} = \sqrt{t_{11}t_{22}}$, $U_{12} = \sqrt{U_{11}U_{22}}$ and $K_1/K_2 = \sqrt{U_{11}/U_{22}}$. We have used $\varepsilon_2 - \varepsilon_1 = 24$ eV, $U_{11} = 13$ eV, $U_{22} = 10$ eV, $K_1 = -8$ eV, $t_{11} = -0.5$ eV and $t_{22} = -0.8$ eV.

Free atom

To study the breathing effect, we first consider a free atom, setting $t_{11} = t_{12} = t_{21} = t_{22} = 0$ in Eq. (S1). We put two electrons on one site and write down the wavefunction

$$|\Phi\rangle = \left[a_{11} c_{11\uparrow}^{\dagger} c_{11\downarrow}^{\dagger} + a_{12} (c_{11\uparrow}^{\dagger} c_{12\downarrow}^{\dagger} + c_{12\uparrow}^{\dagger} c_{11\downarrow}^{\dagger}) + a_{22} c_{12\uparrow}^{\dagger} c_{12\downarrow}^{\dagger} \right] |\text{vac}\rangle \quad (\text{S3})$$

$$= b^2 \tilde{c}_{11\uparrow}^{\dagger} \tilde{c}_{11\downarrow}^{\dagger} |\text{vac}\rangle + \left(a_{22} - \frac{a_{12}^2}{a_{11}} \right) c_{12\uparrow}^{\dagger} c_{12\downarrow}^{\dagger} |\text{vac}\rangle$$

Apart from the last term, we have replaced the 3d orbital by an expanded orbital described by $\tilde{c}_{11\sigma}^{\dagger}$

$$\tilde{c}_{11\sigma}^{\dagger} = \frac{1}{b} \left(\sqrt{a_{11}} c_{11\sigma}^{\dagger} + \frac{a_{12}}{\sqrt{a_{11}}} c_{12\sigma}^{\dagger} \right), \quad (\text{S4})$$

where $b^2 = a_{11} + a_{12}^2/a_{11}$. The coefficients are shown in Table SI. The table illustrates that the last term in

TABLE SI: Coefficients of the wave function in Eq. (S3) for the isolated atom.

a_{11}	a_{12}	$a_{22} - a_{12}^2/a_{11}$
0.91	0.29	-0.01

Eq. (S3) is indeed very small, and the single-determinant with doubly-occupied extended orbital is an adequate description. The breathing lowers the energy cost of double occupancy and renormalizes the effective U_{eff} .

Dimer

We now turn to the full Cu_2 model. Table SII below shows the singlet-triplet splitting. It illustrates how the inclusion of the integral K strongly increases the splitting, due to breathing effects. To understand the results better, we consider a simpler model within only three determinants for the singlet state.

$$\begin{aligned} |1\rangle &= \frac{1}{\sqrt{2}} (c_{11\uparrow}^\dagger c_{21\downarrow}^\dagger + c_{21\uparrow}^\dagger c_{11\downarrow}^\dagger) |\text{vac}\rangle \\ |2\rangle &= \frac{1}{\sqrt{2}} (c_{11\uparrow}^\dagger c_{11\downarrow}^\dagger + c_{21\uparrow}^\dagger c_{21\downarrow}^\dagger) |\text{vac}\rangle \\ |3\rangle &= \frac{1}{2} (c_{11\uparrow}^\dagger c_{12\downarrow}^\dagger + c_{12\uparrow}^\dagger c_{11\downarrow}^\dagger + c_{21\uparrow}^\dagger c_{22\downarrow}^\dagger + c_{22\uparrow}^\dagger c_{21\downarrow}^\dagger) |\text{vac}\rangle, \end{aligned} \quad (\text{S5})$$

where $|\text{vac}\rangle$ is the vacuum state with no electrons. These basis states are shown schematically in Fig. S5. State $|1\rangle$ corresponds to d^9 - d^9 state mentioned in the main text, while $|2\rangle$ and $|3\rangle$ resemble d^8 - d^{10} state in the main state without and with 4d occupation respectively. Hamiltonian (S1) within the basis given by Eq. (S5) reads

$$H = \begin{pmatrix} 2\varepsilon_1 & 2t_{11} & \sqrt{2}t_{12} \\ 2t_{11} & 2\varepsilon_1 + U_{11} & \sqrt{2}K_1 \\ \sqrt{2}t_{12} & \sqrt{2}K_1 & \varepsilon_1 + \varepsilon_2 + U_{12} \end{pmatrix} \quad (\text{S6})$$

Diagonalizing this matrix, we obtain the second column of in Table SII. These results agree rather well with the full calculation for the model in Eq. (S1), although the basis set in Eq. (S5) is incomplete. The splitting is smaller because the higher states have been neglected.

TABLE SII: Triplet-singlet splitting without ($K_1=0$) and with breathing. All values in eV.

K_1	exact, Eq. (S1)	Eq. (S6)
0	0.077	0.076
-8	0.176	0.167

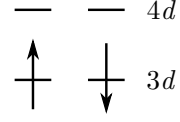


FIG. S4: Schematic representation of the Cu_2 dimer with 3d and 4d levels.

We can now use Löwdin folding, focusing on the upper 2×2 corner of $(z - H)^{-1}$

$$(z - H)^{-1} = \begin{pmatrix} z - 2\varepsilon_1 - 2t_{12}^2/\Delta E & 2t_{11} - 2t_{12}K_1/\Delta E \\ 2t_{11} - 2t_{12}K_1/\Delta E & U_{11} - 2K_1^2/\Delta E \end{pmatrix}^{-1} \quad (\text{S7})$$

where $\Delta E = \varepsilon_2 - \varepsilon_1 + U_{12}$ and we have introduced the approximation $z \approx 2\varepsilon_1$ at some places. The matrix in Eq. (S7) shows rather clearly that there is an interference between breathing and hopping from the 3d orbital on one site to the 4d orbital on the other site. The effective value of U has now been reduced

$$U_{11} \rightarrow U_{11}^{\text{eff}} \equiv U_{11} - 2\frac{K_1^2}{\Delta E} \quad (\text{S8})$$

and the effective hopping has been increased

$$t_{11} \rightarrow t_{11}^{\text{eff}} \equiv t_{11} - 2\frac{t_{12}K_1}{\Delta E}, \quad (\text{S9})$$

since $K_1 < 0$ and t_{11} and t_{12} have the same sign. For the triplet case the basis state $|2\rangle$ does not exist, and these renormalization effects are not present. The singlet-triplet splitting is then

$$E_T - E_S \approx \frac{4(t_{11} - t_{12}K_1/\Delta E)^2}{U_{11} - 2K_1^2/\Delta E} \equiv 4\frac{(t_{11}^{\text{eff}})^2}{U_{11}^{\text{eff}}}. \quad (\text{S10})$$

This illustrates the importance of the renormalization of U_{11} and t_{11} .

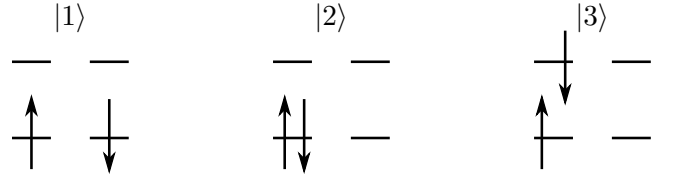


FIG. S5: Schematic representation of states in Eq. (S5) for the dimer model.

HOPPING FOR Cu_2O MODEL

Fig. S6 illustrate hopping possibilities for the singlet and triplet state in a Cu_2O model with nondegenerate levels on Cu (3d) and O (2p). For the triplet case the hopping possibilities are severely limited. In this model J is given by

$$J = \frac{4t_{\text{eff}}^2}{(U_{\text{eff}} + \Delta)^2} \left(\frac{t^2}{U_{\text{eff}}} + \frac{t_{\text{eff}}^2}{U_{\text{eff}} + \Delta} \right), \quad (\text{S11})$$

where U is the 3d – 3d Coulomb integral, t is the hopping from Cu 3d to O 2p and Δ is the energy difference between the Cu 3d orbital and the O 2p orbital. In a model with 4d orbitals on the Cu atoms, t is renormalized to t_{eff} and U to U_{eff} .

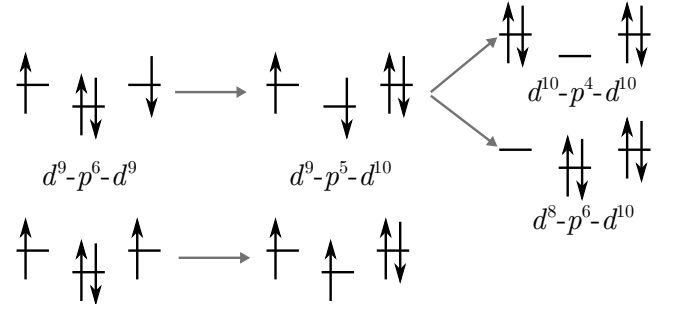


FIG. S6: Schematic representation of the Cu_2O model with Cu 3d and O 2p levels. The O atom is the bridging atom. The upper (lower) part of the figure illustrate available configurations for the singlet (triplet) state.